CRISPR targeting of H3K4me3 activates gene expression and unlocks centromere-proximal crossover recombination in Arabidopsis

Jenia Binenbaum[1,*], Vanda Adamkova[1,*], Hannah Fryer[1], Linhao Xu[1], Nicola Gorringe[1], Piotr Włodzimierz[1,2], Robin Burns[1], Ashot Papikian[3,4], Steven E. Jacobsen[3,5], Ian R. Henderson[1], C. Jake Harris[1,#]

[1] Department of Plant Sciences, University of Cambridge, Cambridge CB2 3EA, UK.
[2] Current Address: Institute of Biochemistry and Biophysics, Polish Academy of Sciences, Warsaw, Poland.
[3] Department of Molecular, Cell and Developmental Biology, University of California, Los Angeles, CA, USA.
[4] Current Address: Plant Molecular and Cellular Biology Laboratory, Salk Institute for Biological Studies, La Jolla, CA 92037, USA.
[5] Howard Hughes Medical Institute, University of California, Los Angeles, CA, USA.
* These authors contributed equally.
[#] For correspondence: cjh92@cam.ac.uk

ABSTRACT

H3K4me3 is a fundamental and highly conserved chromatin mark across eukaryotes, playing a central role in many genome-related processes, including transcription, maintenance of cell identity, DNA damage repair, and meiotic recombination. However, identifying the causal function of H3K4me3 in these diverse pathways remains a challenge, and we lack the tools to manipulate it for agricultural benefit. Here we use the CRISPR-based SunTag system to direct H3K4me3 methyltransferases in the model plant, *Arabidopsis thaliana*. Targeting of SunTag-SDG2 activates the expression of the endogenous reporter gene, *FWA*. We show that SunTag-SDG2 can be employed to increase pathogen resistance by targeting the H3K4me3-dependent disease resistance gene, *SNC1*. Meiotic crossover recombination rates impose a limit on the speed with which new traits can be transferred to elite crop varieties. We demonstrate that targeting of SunTag-SDG2 to low recombining centromeric regions can significantly stimulate proximal crossover formation. Finally, we reveal that the effect is not specific to SDG2 and is likely dependent on the H3K4me3 mark itself, as the orthogonal mammalian-derived H3K4me3 methyltransferase, PRDM9, produces a similar effect on gene expression with reduced off-target potential. Overall, our study supports an instructive role for H3K4me3 in transcription and meiotic recombination and opens the door to precise modulation of important agricultural traits.

INTRODUCTION

Re-programming of transcriptional landscapes in response to developmental and environmental cues critically underlies a plant's ability to adapt and optimise its performance. The potential to re-wire and fine-tune expression of endogenous genes therefore holds great promise for agricultural improvement. Chromatin modifications associated with gene expression play an essential role in this process [1].

Trimethylation of histone 3 lysine 4 (H3K4me3) is a well-studied and highly conserved chromatin mark. H3K4me3 enrichment around the transcriptional start site of expressed genes is observed across eukaryotes [2], and is thought to assist in transcriptional maintenance and memory of cell identity [3]. Despite the ubiquity of H3K4me3 and its positive correlation with gene expression, whether this chromatin mark plays an instructive role in transcription remains a matter of debate, due in part to the limited evidence of transcriptional impact when H3K4me3 levels are perturbed [4,5]. In animals, TAF3 directly binds to H3K4me3 and recruits basal transcription factor machinery, providing a plausible mechanism to stimulate transcription [6,7]. Recent work in embryonic stem cells shows that H3K4me3 plays a role in RNA Polymerase II pause-release and elongation, rather than transcriptional initiation [8]. In plants, there are no TAF3 homologues and whether similar mechanisms exist to promote transcription downstream of H3K4me3 remains unknown [9–13].

H3K4me3 also plays a key role in several other genome-related processes. For instance, meiotic recombination, which allows for genetic exchange between parental chromosomes [14]. This process is essential for breeders to transfer traits from wild relatives into elite cultivars [15,16]. However, the positioning of meiotic recombination events is non-uniform across the genome, with gene-rich chromosomal arms having relatively higher rates of crossover recombination, and centromeric repeat-rich regions being more recombination-suppressed [17,18]. Loci encoding desirable traits that reside within these low-recombining regions of the genome can show linkage drag with deleterious variants during traditional breeding approaches, which limits genetic gains [15,16]. In mammals, the H3K4me3 SET domain methyltransferase containing protein, PRDM9, helps to define active sites of crossover recombination [19]. While H3K4me3 levels are positively correlated with recombination rates in plants [17,20], whether

deposition of H3K4me3 is sufficient to promote crossover formation is entirely unknown.

One way to reveal the causal role of an epigenetic modification is to directly deposit the mark at targeted genomic locations [21–25]. Epigenome editing tools, such as the CRISPR-based SunTag system [26], have proven to be highly efficient at targeting DNA methylation addition, removal and histone modification [23,27–32], although their utility for modulating agronomically useful traits is only just beginning to be realised [33], and is limited by the range of possible marks that can be directed [1]. In the model plant *Arabidopsis thaliana*, SDG2 is the main histone methyltransferase responsible for deposition of H3K4me3 [34]. Here, we describe CRISPR directed H3K4me3 deposition in plants and demonstrate its utility in a range of scenarios. We translationally fuse the SDG2 methyltransferase domain to the scFv single chain antibody, which can be recruited to the SunTag epitope chain connected to a dead Cas9 (dCas9). We show that SunTag-SDG2 mediated H3K4me3 deposition can activate the transcription of endogenous genes. Further, by targeting a disease resistance gene, we generate plants with enhanced resistance capabilities. Next, we show that SunTag:SDG2 can unlock meiotic crossover recombination in centromere-proximal regions. Finally, we incorporate the methyltransferase domain from PRDM9 into SunTag - which was recently shown to instruct transcription in a mammalian context [31] - showing that it is also highly efficient for transcriptional activation in plants, and displays reduced off-target potential. These results demonstrate the power and versatility of a functional H3K4me3 targeting system for modulation of critical genome templated processes, such as transcriptional enhancement and meiotic recombination.

RESULTS

SunTag SDG2 mediates transcriptional activation of *FWA*

The SunTag system we chose is composed of three components [26,35] (Fig. 1A): 1) A catalytically deactivated (nuclease deficient) Cas9 (dCas9) translationally fused to a tail with 10x copies of the GCN4 epitope, each separated by a 22 amino acid flexible linker. 2) An effector module that encodes a single chain fragment variable (scFv) antibody that recognises GCN4, super folder GFP (sfGFP), and the effector of interest (e.g. enzymatic modifier / recruitment scaffold). 3) *U6* promoter driven CRISPR guide RNA. When the three components are expressed within the same cell, the guide RNA recruits the dCas9-10xGCN4 to the target locus of interest, while the GCN4 single chain antibody containing effector module binds to the dCas9-10xGCN4 epitope tail. The system allows for conformational flexibility and the potential for high stochiometric concentration of the effector at the locus of interest.

We inserted the C-terminal coding sequence of the H3K4 methyltransferase, SDG2 (amino acids 1571-2335), into the SunTag system (Fig. 1B, Supp. Fig. S1). As a control, we also generated a version of SDG2 with an amino acid change (Y1903F) predicted to abolish catalytic activity (Supp. Fig. S2) [34,36]. Hereafter, we refer to these as SDG2 and dSDG2 (for catalytically deactivated). We targeted the SunTag system to the promoter of the epigenetically repressed *FWA* gene [37], using the previously published CRISPR guide RNA 4, which is complementary to two tandem repeat regions directly upstream of the *FWA* transcription start site (TSS) [29]. These were transformed into the *rdr6* background, as previous results have shown that SunTag is less prone to silencing and achieves higher transgene expression [27]. We observed that SunTag:SDG2:FWA_g4 activated *FWA* mRNA expression, while the SunTag:dSDG2:FWA_g4 and no guide RNA (SunTag:SDG2:No_g) controls did not (Fig 1C, Supp. Fig. 1C). Importantly, effector module expression was detected in all constructs, indicating that both guide RNA targeting and catalytic activity are required for *FWA* activation (Supp. Fig 3A). To validate the presence of the SunTag and test for the deposition of H3K4me3, we performed ChIP qPCR and observed significant enrichment both for the presence of SunTag and for H3K4me3 accumulation at the target site in these transgenic lines (Fig. 1D and Sup Fig 3B), confirming that SunTag-

130 SDG2 binds the *FWA* locus and deposits H3K4me3. To investigate
131 SunTag:SDG2:FWA_g4 binding genome-wide, we performed high-throughput
132 sequencing (anti-HA ChIP-seq; the HA-tag is present on both the dCas9 and effector
133 fusion modules), which confirmed the previously reported high specificity of SunTag
134 targeting [28], with the *FWA* target locus as the most enriched binding target (Fig. 1E,
135 Supp. Fig. 4). Only 3 conserved binding sites were identified in the
136 SunTag:SDG2:FWA_g4 lines; *FWA* and two off-target sites previously identified as
137 having sequence-similarity to FWA_g4 [28]. Furthermore, transcriptome analyses
138 confirmed *FWA* as the highest fold change differentially upregulated gene (Fig. 1F).
139 Together, these data indicate that deposition of H3K4me3 by SunTag:SDG2 is
140 sufficient to overcome epigenetic silencing and drive transcriptional activation in a
141 locus-specific manner.
142
143 Next, to examine the genome-wide effect on H3K4me3 by SunTag-SDG2 we
144 performed ChIP-seq analysis, confirming enrichment at the *FWA* locus and canonical
145 genic H3K4me3 patterning (Fig 1E, Supp. Fig. 5). In addition to a modest peak at the
146 +1 nucleosome at *FWA*, the H3K4me3 signal extended into the gene body. Performing
147 metaplots over genes, transcriptional start sites (TSS's), and endogenous H3K4me3
148 peaks, we observed that SunTag:SDG2 lines generally display a moderate increase
149 of H3K4me3 over the 3' end of gene bodies (Fig. 1G). Correspondingly, we observed
150 reduced H3K4me3 signal at endogenous peaks and TSS regions (Fig. 1G). As the
151 H3K4me3 peak at *FWA* in our SunTag:SDG2:FWA_g4 lines was not as strong as that
152 observed for *fwa* in the epiallelic state [27,38], we asked whether the effect could persist
153 in the next generation. Analysis of T_2 seedlings from two independent lines
154 segregating for the presence of SunTag:SDG2:FWA_g4 showed that *FWA* activation
155 was entirely dependent on the presence of the transgene (Supp. Fig. 6). Together
156 these data indicate that while SunTag:SDG2:FWA_g4 can site-specifically activate
157 *FWA* expression, it is insufficient to overcome the endogenous silencing machinery as
158 required to switch *FWA* into the stably active *fwa* epiallelic state [32,39].

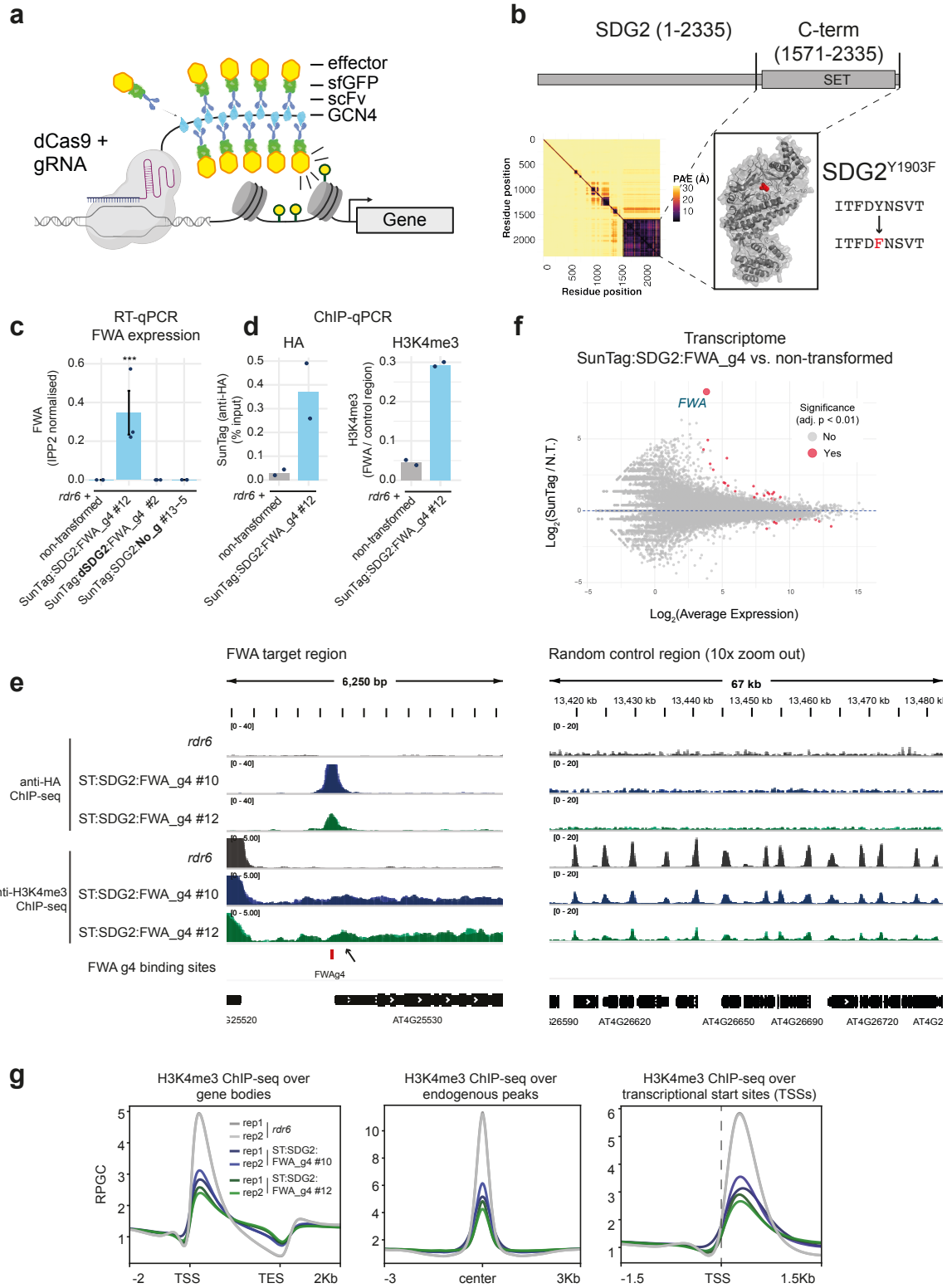

Figure 1: SunTag:SDG2 activates *FWA* mRNA expression.

A) Schematic showing the SunTag system for modulation of chromatin [28,35]. Created in BioRender. Harris, J. (2025) https://BioRender.com/mqs3hbr. B) Upper panel shows SDG2

with catalytic SET domain (drawn approximately to scale). Lower left depicts predicted alignment error (PAE) plot from AlphaFold3 [75] prediction of the SDG2 coding sequence with a box drawn around the region cloned into SunTag (amino acids 1571-2335). Lower right depicts the AlphaFold3 model for $SDG2_{1571-2335}$, with the position of the amino acid change (Y1903F) for dSDG2 indicated (shown in red). C) RT-qPCR for *FWA* expression from the genotypes indicated. Error bars represent SEM from three biological replicates (a pool of 10 seedlings) from the lines (#) and genotypes indicated. *** indicates $p < 0.005$ (ANOVA with post-hoc Tukey HSD. D) ChIP qPCR for the presence of SunTag (left panel) and H3K4me3 enrichment (right panel) over the TSS of *FWA*. The control region (AT5G65130) used for normalisation has high H3K4me3. E) Genome browser images showing ChIP-seq enrichment of SunTag (anti-HA) and H3K4me3 levels of two independent SunTag:SDG2:FWA_g4 lines (2 biological replicates each, bio replicate tracks are overlaid) at the *FWA* TSS (left panel) and at a random genic control region. F) MA plot comparing the transcriptome of SunTag:SDG2:FWA_g4 as compared to the non-transformed control (*rdr6*). Differentially expressed genes were defined using an adjusted p-value (Bonferroni method), shown in red (FDR < 0.01), with *FWA* labelled and enlarged for visibility. G) H3K4me3 ChIP-seq metaplots over all genes, H3K4me3 endogenous peaks, and TSS regions.

SNC1 **mediated modulation of disease resistance**

Given that SunTag:SDG2 can modulate chromatin and activate *FWA* gene expression, we were interested use the tool to modify an important plant trait. Gene expression during pathogen attack is a key factor in determining disease outcome. *SNC1* is disease resistance gene, encoding a nucleotide-binding leucine-rich repeat protein [40] that is located within the partially epigenetically repressed *RPP5* gene cluster [41–43]. *SNC1* expression activity is modulated by H3K4me3 [44], and its level of expression is positively correlated with basal resistance [41,44]. Therefore, *SNC1* is an attractive target for proof-of-principle modulation of disease resistance by epigenome engineering.

We designed guide RNAs to target the promoter region of *SNC1* directly upstream of the TSS and inserted it into our SunTag:SDG2 and SunTag:dSDG2 constructs (Fig. 2A, Supp. Fig 7). As high pathogen resistance is generally associated with dwarfed plants, we inspected the lines for growth and developmental phenotypes. In our *SNC1* targeting SunTag:SDG2, but not our SunTag:dSDG2 control, we observed small, dwarfed phenotype with reduced rosette surface area (Fig. 2AB, Supp. Fig 7). These

198 plant phenotypes resembled those of our positive control *bal* lines, which overexpress
199 *SNC1*, resulting in the small dwarfed plant phenotype and high basal disease
200 resistance [41]. As the phenotype is consistent with upregulation of *SNC1* by SunTag,
201 we confirmed the increased expression and successful targeting of SunTag:SDG2 to
202 the *SNC1* locus (Fig. 2CD, Supp. Fig 7).
203
204 To assess whether these lines show increased pathogen resistance, we challenged
205 the plants with the generalist plant pathogen, *Pseudomonas syringae* pathovar *tomato*
206 strain DC3000 (*Pst*). The recently described bioluminescent *Pst* (*Pst::LUX*) was used
207 to allow for non-destructive quantification of pathogen colonisation [45]. We developed
208 a high-throughput assay system, inoculating 7-day-old seedlings with *Pst::LUX* and
209 imaging to quantify the levels of *Pst::LUX* at 24 hour intervals over the course of
210 infection. We challenged a range of control genotypes that are known to be *Pst* hyper-
211 resistant (*bal*), constitutively primed (*edr1*), and susceptible (*NahG*), recapitulating the
212 expected pattern of *Pst::LUX* colonisation dynamics in these backgrounds (Supp. Fig.
213 S8) [45]. Next, we challenged our *SNC1* targeting lines with *Pst::LUX*, finding that they
214 displayed hyper-resistance that was nearly identical in magnitude to that of the *SNC1*
215 overexpressing positive control, *bal* (Fig. 2E, Supp. Fig. 7). The results demonstrate
216 that epigenome-engineering of a single defense gene, *SNC1*, is sufficient to generate
217 plants with improved disease resistance phenotypes in Arabidopsis.
218

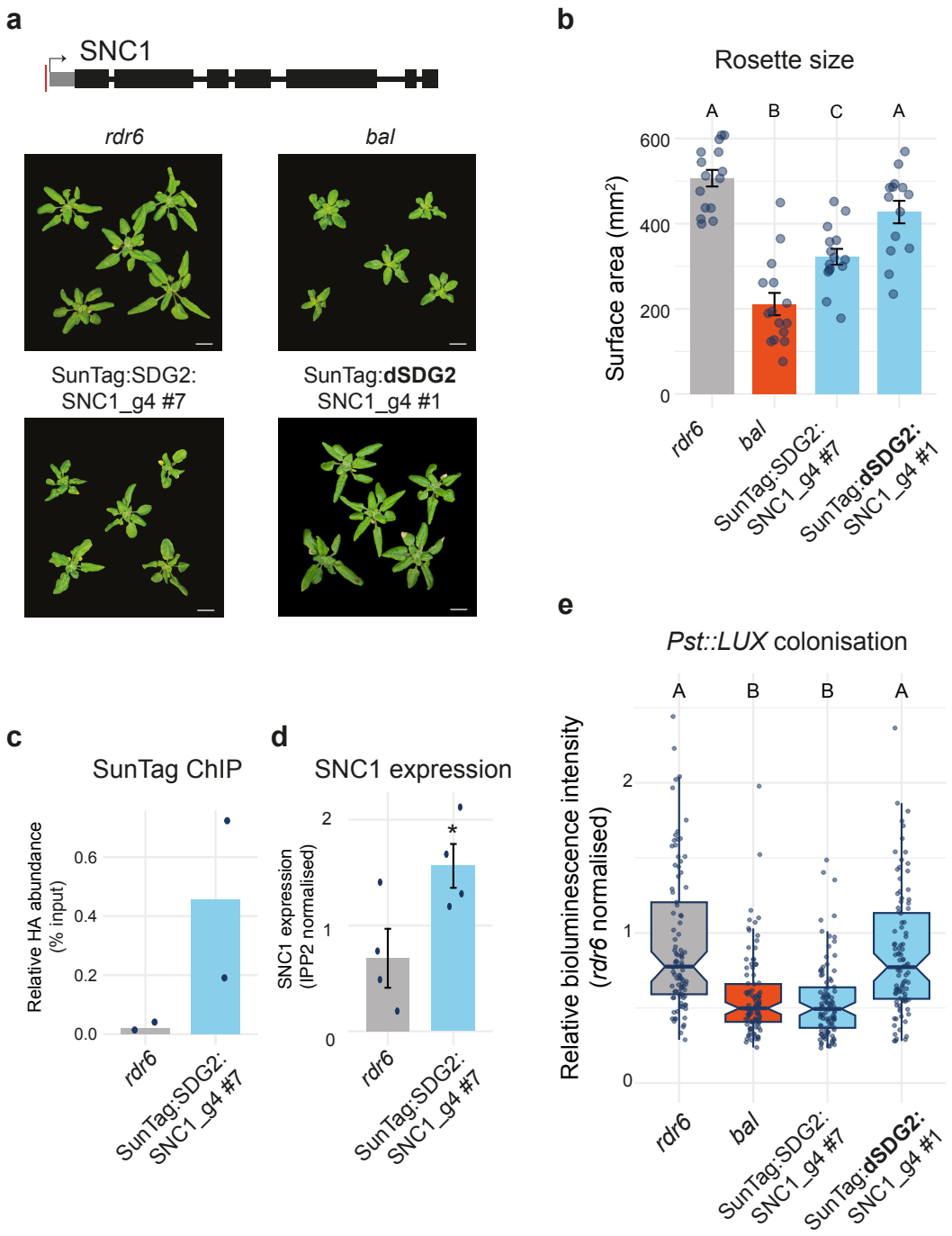

Figure 2: SunTag:SDG2 targeting to *SNC1* enhances resistance to *P. syringae*. A) Upper, schematic of the *SNC1* gene, with the red line indicating the *SNC1* gRNA target site, drawn to scale. Lower, representative images of 3-week old plants from the genotypes indicated. Scale bar = 1cm. B) Rosette size quantification. Each dot represents an individual plant. Error bars represent SEM. Different letters indicate significant difference by ANOVA with post-hoc Tukey HSD, $p < 0.05$. n = 14 for SunTag:dSDG2:SNC1_g4 #1, n = 15 for the rest. C) ChIP qPCR for the presence of SunTag at SNC1. D) RT-qPCR for *SNC1* expression. Error

227 bars represent SEM. * indicates p-value = 0.045 by student's *t*-test. n = 4 biological replicates
228 (each a pool of 10 seedlings). E) *Pst::LUX* assay for colonisation quantification at 3 days post
229 inoculation. Different letters indicate significant difference by ANOVA with post-hoc Tukey
230 HSD, $p < 0.05$. Boxplots show the median, the interquartile range, whiskers extending to 1.5×
231 the interquartile range, and individual data points plotted as dots. n = 96 wells, containing 3
232 seedlings each.
233
234 **Centromeric targeting of SDG2 drives increased meiotic crossover**
235 **recombination**
236
237 Beyond transcription, H3K4me3 is associated with many other fundamental genome
238 related processes including meiotic recombination. In plants, meiotic crossover
239 recombination rates broadly correlate with epigenetic territories and are non-uniform
240 across the genome [17,18]. In *A. thaliana*, recombination occurs at a relatively high
241 frequency in euchromatic arms, whereas it is significantly reduced over the
242 heterochromatic pericentromeric and centromeric [46–48]. Crossover hotspots are often
243 found to be high at gene promoters where H3K4me3 is enriched [20]. In previous work,
244 we showed that gene-associated crossover recombination hotspots can be supressed
245 by small RNA directed DNA methylation [49]. Therefore, we hypothesised that
246 recombination within the centromeric regions might be increased by SunTag mediated
247 epigenetic activation via deposition of H3K4me3.
248
249 The Arabidopsis centromeres are composed of highly repetitive *CEN178* satellite
250 repeat arrays [47,50]. We designed a guide RNA that perfectly matches to 241 target sites
251 within the *CEN178* repeats within the centromeric region of chromosome 3
252 (LRCen3_g), and inserted this guide into the SunTag:SDG2 system. As centromere-
253 proximal crossover recombination events are relatively rare, to quantitatively assess
254 the impact on recombination rate over centromere 3, we crossed (non-transgenic) Col-
255 0 plants with the *CTL3.9* crossover reporter [51]. *CTL3.9* is a transgenic a line that
256 encodes linked T-DNAs that encode red and green fluorescent markers expressed
257 from a seed-specific promoter, that flank *CEN3* [48]. The red and green T-DNA insertions
258 span a region of approximately 8.91 Mb in the Col-CEN assembly of chromosome 3,
259 which contains the centromeric satellite arrays in addition to flanking pericentromeric
260 heterochromatin (Fig. 3A) [48]. Meiotic crossover recombination events that occur within

261 this region result in progeny inheriting either red or green fluorescent markers, the
262 frequency of which can be measured by automated seed imaging [52]. We transformed
263 *CTL3.9* F_1 double hemizygous plants with the SunTag:SDG2:LRCen3_g construct
264 (Fig. 3AB). The F_2 plants represented individual transformants of the SunTag (T_1 for
265 SunTag), and so F_3 seeds from individual F_2 plants were imaged to measure the rate
266 of crossover recombination, in centiMorgans, over the centromere 3 spanning region
267 of *CTL3.9* [48].
268
269 Remarkably, the SunTag:SDG2:LRCen3_g containing lines showed significantly
270 elevated crossover recombination within the *CTL3.9* interval as compared to the non-
271 SunTag control lines (ANOVA with post-hoc Tukey HSD cutoff <0.05) (Fig. 3C, Supp.
272 Fig. 9). Some individual transgenic plants displayed a substantial increase in *CTL3.9*
273 crossover recombination rate, with over 50% higher frequency, as compared to the
274 average in non-transgenics, across this megabase-scale centromere-spanning region
275 (Fig. 3C). SunTag:SDG2:LRCen3_g progeny from the most highly recombining line
276 that also showed Mendelian inheritance of the *CTL3.9* T-DNAs was sown to assess
277 whether the effect could persist in the subsequent (F_4) generation. The plants retained
278 a significantly elevated crossover frequency across *CTL3.9* in the next generation,
279 suggesting that the SunTag:SDG2:LRCen3_g effect is relatively stable in the presence
280 of the transgene (Fig. 3C).
281
282 To examine the distribution of SunTag:SDG2:LRCen3_g in the high recombination
283 lines (P4, Supp. Fig. 9), we performed ChIP-seq (anti-HA) comparing progeny from
284 sibling plants that either inherited (+SunTag), or did not inherit (-SunTag) the SunTag
285 machinery, as well as non-transgenic (Col-0) controls. Chromosome-wide plots at 100
286 kb resolution showed that SunTag:SDG2 is enriched over the entire centromeric
287 region of chromosome 3 (Fig. 3D). SunTag was also enriched over the other four *A.*
288 *thaliana* centromeres (Supp. Fig. 10). As these regions are highly repetitive, we
289 reasoned that the LRCen3 guide RNA might additionally bind the other centromeres
290 due to mismatch tolerance. Indeed, while the LRCen3 guide RNA aligns perfectly to
291 250 loci within the centromere of chromosome 3, by allowing a single mismatch the
292 guide is predicted to bind to target sites in all 5 centromeres (Supp. Fig. 11), which is
293 consistent with the ChIP-seq data observed. Having confirmed that SunTag is
294 enriched within the centromeric regions in these lines, we next examined levels of

295 H3K4me3. Inspecting centromeric regions, we observed many instances of novel or
296 elevated H3K4me3 peaks in the LRCen3 targeted lines (Supp. Fig. 12). Quantifying
297 H3K4me3 levels at these peaks confirmed the enrichment of H3K4me3 levels over
298 the centromere region and further extending into the neighbouring pericentromeres
299 (Fig. 3D, Supp. Fig. 13). As the markers on *CTL3.9* span the centromere and adjacent
300 pericentromeric regions [48] (Fig. 3D), this is consistent with the significantly elevated
301 crossover recombination rate observed. Overall, the results demonstrate that
302 centromerically targeted SunTag-SDG2 can elevate the meiotic crossover potential of
303 these typically recombination-suppressed regions.

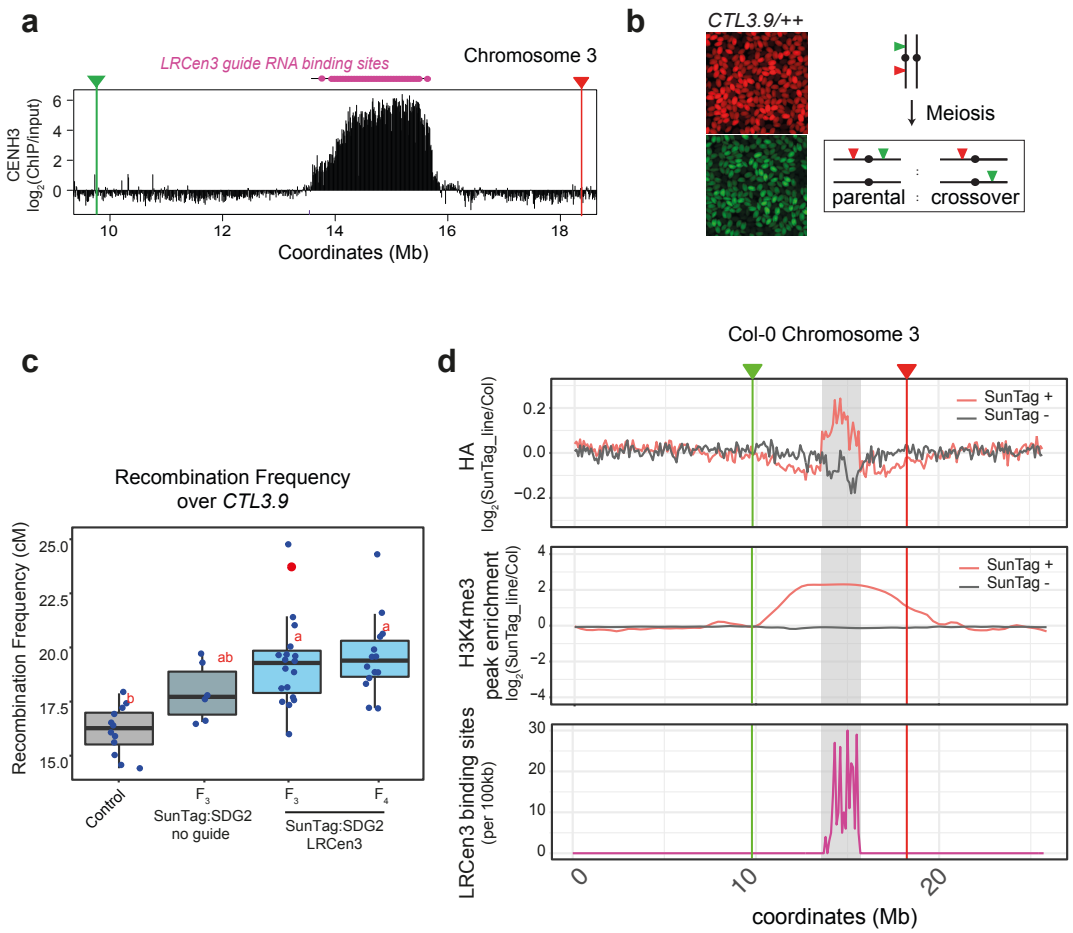

304
305

306 **Figure 3: Centromeric targeting of SunTag:SDG2 elevates meiotic crossover**
307 **recombination rate.**
308 A) Region of chromosome 3, showing CENH3 ChIP-seq enrichment [50] with *CTL3.9* [51] red /
309 green T-DNA marker positions and LRCen3 guide RNA binding sites indicated. B) Left panel,

310 representative image of red and green fluorescing seeds from a *CTL3.9* double homozygous
311 line. Right panel, schematic of showing how crossovers are identified within *CTL3.9*. C)
312 Boxplot showing crossover recombination frequency over *CTL3.9* in centiMorgans. Control
313 data is from Col-0 (non-transgenic) crossed to *CTL3.9*. Different letters indicate significant
314 difference by ANOVA with post-hoc Tukey HSD ($p<0.05$). Control: n = 12, LRCen3 F3: n = 19,
315 No guide: n = 6, LRCen3 F4: n = 14. Boxplots show the median, the interquartile range,
316 whiskers extending to 1.5× the interquartile range, and individual data points plotted as dots.
317 The red dot indicates the seed set line taken to the next generation (F_4). D) Chromosome-
318 wide plots of chromosome 3. Upper panels shows enrichment of SunTag (anti-HA) by ChIP-
319 seq in sibling lines with / without SunTag (+/-). Enrichment is calculated as $\log_2$ fold-change
320 over non-transgenic (Col-0) controls in 100 kb windows. Middle panel shows H3K4me3
321 enrichment over H3K4me3 peaks ($\log_2$ fold-change over non-transgenic (Col-0) controls). The
322 lower panel depicts an LRCen3 guide RNA binding site density over chromosome 3. *CTL3.9*
323 marker positions are indicated, and centromeric regions are shown in grey. All data are
324 mapped the Col-CEN genome assembly [47].
325
326 **Mammalian PRDM9 drives efficient transcriptional activation in Arabidopsis**
327
328 As the enrichment of H3K4me3 in SunTag:SDG2:LRCen3_g was not exclusive to the
329 guide RNA targeted centromeric regions, we reasoned that the SunTag system may
330 afford some level of off-target activity due to non-guide RNA directed ectopic
331 interactions. Consistent with this observation, we also noticed that our SunTag:SDG2
332 no guide RNA controls frequently exhibited pleotropic developmental phenotypes
333 (Supp. Fig. 14). To quantify global levels of H3K4me3, we performed bulk histone
334 westerns, comparing no guide RNA lines to *FWA* expression-activating guide RNA
335 containing lines. Importantly, the SDG2 effector itself is expressed to similar levels as
336 in the *FWA* targeting lines (Supp. Fig. S3a). The SunTag:SDG2 no guide lines all
337 showed significant (3-4 fold) increases in global levels of H3K4me3, as compared to
338 the *FWA* guide containing lines (Supp. Fig. 15A). This indicates that the presence of
339 the guide RNA may enhance the targeting specificity of the SunTag complex by
340 reducing the frequency of non-specific interactions that result in off-target deposition
341 of H3K4me3. We also observed that a small number of SunTag:dSDG2:FWA_g4 lines
342 could activate *FWA* expression, but this effect was limited to lines where the dSDG2
343 effector was highly overexpressed (Supp. Fig. 15B). To systematically examine this
344 effect, we screened T_1 plants finding that 6% (1/16) of the *FWA* targeted dSDG2, and

345 14% (2/16) of the no guide SDG2 lines could activate *FWA* expression (Supp. Fig. 16).
346 This underscores the potential off-target effects from SunTag:SDG2, and suggests that
347 dSDG2 either retains some residual catalytic activity, or that it can recruit endogenous
348 machinery to initiate transcription independently of H3K4me3 deposition.
349
350 In order to reduce off-target activity and the potential for co-recruitment of endogenous
351 complexes, we replaced SDG2 with an orthogonal effector, PRDM9. PRDM9 is a
352 mammalian H3K4me3 methyltransferase, and Policarpi *et al.,* (2024) recently showed
353 that the catalytic domain could be incorporated into the SunTag system for targeting
354 of H3K4me3 in mammalian cells. Therefore, we inserted the PRDM9
355 methyltransferase domain, as well as a catalytically deactivated version, into our
356 SunTag system and targeted *FWA* (Fig. 4A). Strikingly, SunTag:PRDM9:FWA_g4 was
357 highly effective at activating *FWA* mRNA expression (Fig. 4B). In the T_1 generation,
358 72% (23/32) of SunTag:PRDM9:FWA_g4 plants could activate FWA, while no of plants
359 with the dPRDM9 (0/16), or no-guide RNA (0/19) constructs were able to do so (Supp.
360 Fig. 17). Importantly, we could detect robust expression of the effector from all
361 constructs (Supp. Fig. 11). ChIP qPCR confirmed the presence of SunTag and the
362 enrichment of H3K4me3 at *FWA* (Fig 4C). At the transcriptome level, the effect of
363 SunTag:PRDM9:FWA_g4 was highly specific, with only 19 genes identified as
364 differentially expressed (15 up, 4 down, FDR<0.01), and with *FWA* itself having the
365 highest fold change amongst them (>158 fold change over *rdr6*) (Fig. 4D). Unlike the
366 no-guide SDG2 transgenic lines, bulk histone westerns confirmed no H3K4me3
367 increases in the PRDM9 no-guide lines (Supp. Fig. 18). Correspondingly we did not
368 observe any developmental defects and saw only minor transcriptional defects when
369 comparing the no-guide lines to non-transformed *rdr6* controls (Supp. Fig. 19). Finally,
370 we performed ChIP-seq in these lines, confirming *FWA* as the most significant and
371 enriched peak for SunTag binding and revealing deposition of H3K4me3 at the
372 transcriptional start site of *FWA* (Fig. 4E).
373
374 At the genome-wide level, while SunTag:PRDM9:FWA_g4 lines also displayed modest
375 decrease in H3K4me3 signal at endogenous peaks with a corresponding increase
376 over 3′ gene body regions (Fig. 4F, Supp. Fig. 20), these effects were less pronounced
377 than SunTag:SDG2 (Fig. 1G), again suggesting that the PRDM9 effector fusion has
378 reduced off-target potential. Finally, we performed the *CTL3.9* meiotic recombination

assay, finding that PRDM9 was similarly effective at increasing crossover frequency over the centromeric *CTL3.9* interval (Fig. 4G, Supp. Fig. 21). Overall, our results demonstrate that PRDM9 is highly effective for deposition of H3K4me3 in plant, as well as mammalian SunTag systems. Furthermore, as PRDM9 is not likely to have endogenous partners in the plant nucleus, the results provide strong evidence in favour of a direct role for H3K4me3 in transcriptional stimulation.

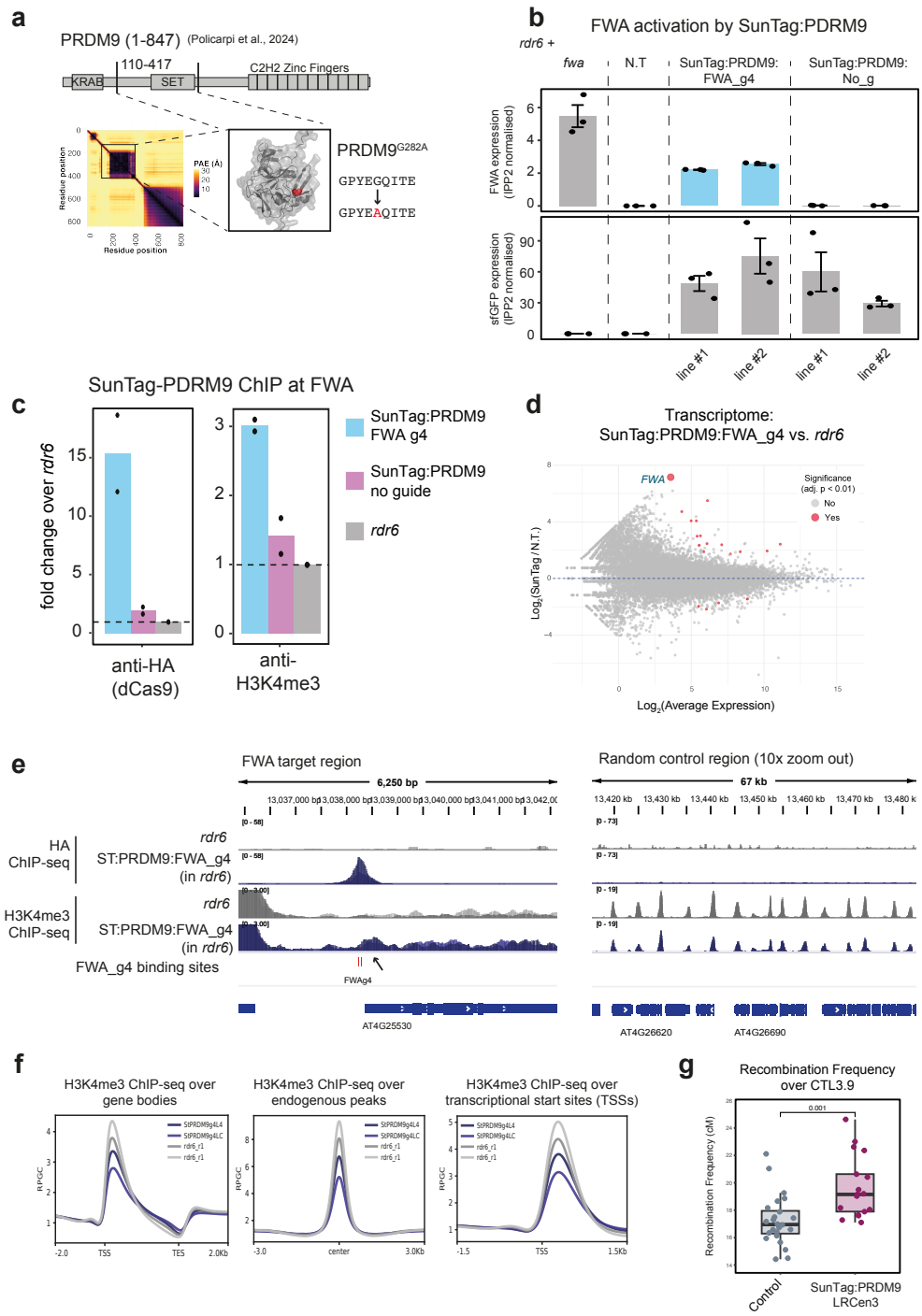

386

387 **Figure 4: SunTag PRDM9 is sufficient for activation of *FWA*.**

388 A) Upper panel shows PRDM9 with catalytic SET domain (drawn approximately to scale).
389 Lower left depicts predicted alignment error (PAE) plot from AlphaFold3 prediction of the
390 PRDM9 coding sequence with a box drawn around the region cloned into SunTag (amino
391 acids 110-417). Lower right depicts the AlphaFold3 model for $PRDM9_{110-417}$, with the amino
392 acid change for dPRDM9 indicated (position shown in red). B) RT-qPCR for *FWA* (upper
393 panel) and the effector module (sfGFP, lower panel) for the genotypes indicated. Dots
394 represent individual plants, with two independent T_3 lines used per construct, 3 biological
395 replicates per construct. Error bars represent SEM. C) ChIP qPCR for the presence of SunTag
396 (left panel) and H3K4me3 enrichment (right panel) over the TSS of *FWA*. D) MA plot
397 comparing the transcriptome of SunTag:PRDM9:FWA_g4 as compared to the non-
398 transformed control (*rdr6*). Differentially expressed genes were defined using an adjusted p-
399 value (Bonferroni method), shown in red (FDR < 0.01), with FWA labelled and enlarged for
400 visibility. E) Genome browser image showing efficient SunTag targeting and H3K4me3
401 enrichment at *FWA* and at a random genic control region. Biological replicate tracks from
402 independent lines are overlaid. F) H3K4me3 ChIP-seq metaplots over all genes, H3K4me3
403 endogenous peaks, and TSS regions. G) Boxplot showing crossover recombination frequency
404 over *CTL3.9* in centiMorgans (p<0.001, two-sample, two-sided t-test). Boxplots show the
405 median, the interquartile range, whiskers extending to 1.5× the interquartile range, and
406 individual data points plotted as dots. n = 24 for control, n = 17 for Suntag:PRDM9 LRCen3.

407

408 **DISCUSSION**

409 Our results demonstrate that targeted deposition of H3K4me3 using the SunTag
410 system enables transcriptional activation, enhanced pathogen resistance, and
411 increased crossover recombination over megabase-scale centromere-proximal
412 regions. These findings support an instructive role for H3K4me3 in transcriptional
413 control and open new avenues for precise, potentially non-GM crop improvement
414 through epigenome engineering. Because the effect depends on the presence of a
415 functional catalytic domain, and is observed using both native and non-native
416 methyltransferases, it is unlikely to result from co-recruitment of endogenous
417 complexes, strengthening the argument that H3K4me3 itself can act as a causal
418 regulatory mark.

419 In a related study [38] showed that full activation of *FWA* by recruitment of SDG2
420 required active removal of DNA methylation by ROS1 and related proteins. Whether
421 H3K4me3 directly recruits ROS1 machinery is currently unknown. However, the
422 finding that PRDM9 also causes potent transcriptional activation of *FWA* suggests that
423 ROS1 recruitment is downstream of H3K4me3, rather than being co-recruited via
424 COMPASS complex components [9,10,53]. Removal of DNA methylation could also help
425 explain the increased centromeric crossover recombination observed over the *CTL3.9*
426 interval, consistent with prior work showing elevated recombination rates in non-CG
427 DNA methylation mutants in similar interval [48,54]. However, in mammalian systems,
428 H3K4me3 has been shown to stimulate transcription by promoting Pol II pause release
429 [8]. Similarly, using zinc finger-fused SDG2 in *A. thaliana*, the Wang et al 2025 study
430 found many instances of ectopic H3K4me3 driving transcriptional stimulation in the
431 absence of pre-existing or DNA methylation removal. Thus, DNA methylation-
432 independent mechanisms must also play a role H3K4me3 mediated transcriptional
433 activation.

434 In our system, SunTag:SDG2 and PRDM9 targeting of *FWA* with a single guide caused
435 strong upregulation at this locus, yet we did not observe any plants that switched to
436 late-flowering as previously reported when *FWA* transitions to an active *fwa* epistate.
437 The Wang et al, 2025 study only observed flowering delays when two guides were
438 used to target the *FWA* promoter. We cannot exclude the possibility that *FWA* failed
439 to reach a critical expression threshold in our experiments, or that expression was
440 developmentally mis-timed or mis-localised. It is also possible that in the single guide
441 system the H3K4me3 deposition induces more non-functional transcripts, consistent
442 with chromatin's roles in co-transcriptional regulation [55,56]. The lack of a flowering time
443 phenotype also aligns with the absence of transgenerational effects, suggesting that
444 the targeting did not remove sufficient DNA methylation to establish heritable gene
445 *FWA* expression. This is further supported by the modest H3K4me3 peak observed at
446 *FWA* in our targeted lines, compared to lines that have fully switched to late flowering
447 [38].

448 Both mammalian PRDM9 and the endogenous SDG2 catalytic domains were able to
449 transcriptionally activate *FWA* and elevate crossover recombination rates over a
450 recombination-suppressed centromere spanning interval. Seminal work in *Drosophila*

451 *melanogaster* and showed that while loss of the H3K4 monomethyltransferases, *Trr*,
452 was lethal, the corresponding catalytic-null caused only minor developmental defects
453 [57]. This underscores the importance of using catalytic mutations and orthogonal
454 effectors to separate the effects from histone marks themselves, over the histone
455 modifying enzymes and associated complexes. It also highlights the utility of modular
456 targeting platforms that can decouple chromatin modifications from native pathways.
457 Continued development of such tools will be crucial for both basic discovery and
458 applied crop engineering [23,25,27,28,58–66].

459 We observed off-target effects in both SunTag:PRDM9 and SunTag:SDG2 transgenic
460 lines, manifested as increased non-specific H3K4me3 background signal and reduced
461 occupancy at endogenous locations (Fig. 1G, Fig. 4F, Supp. Fig. 13). This off-target
462 signal is inherently difficult to diagnose, as it is virtually indistinguishable from a ChIP-
463 seq with reduced signal-to-noise. However, as we observed the same trend in multiple
464 independent experiments, with the SunTag lines always showing this same pattern as
465 compared to the non-transgenics (Fig. 1G, Fig 4F, Supp. Fig. 13A), we conclude that
466 the effect is due to SunTag off-targeting, rather than ChIP signal variability. Notably,
467 these effects were weaker in PRDM9 lines, supporting the idea that orthogonality
468 reduces off-target potential. Unlike SDG2, PRDM9 lines without guide RNAs did not
469 show elevated bulk H3K4me3 levels (Supp. Fig. 15 vs. 18). The strong developmental
470 phenotypes in the SDG2 no-guide lines (Supp. Fig. S14) may result from
471 transcriptional misregulation at ectopically modified loci, or could be caused by
472 transcription-independent metabolic defects [5]. Interestingly, these phenotypes were
473 largely absent in the SDG2 guide RNA targeted lines, suggesting that the guide RNAs
474 reduce this off-target activity. With the guided lines, it is worth reiterating that the
475 SunTag on-target activity is highly specific for both SDG2 and PRDM9, with *FWA* as
476 the most significantly enriched SunTag peak by ChIPseq, and is the most upregulated
477 transcript with few other DEGs observed (Fig. 1F and Fig. 4D). However, off-target
478 effects and metabolic impacts are important considerations when designing these
479 systems for use in crops, which possess larger genomes and more complex regulatory
480 architectures than *A. thaliana* [67]. Notably, SunTag has already been successfully
481 deployed in rice for precise removal of DNA methylation in the context of cold stress
482 adaptation [60], demonstrating the feasibility and potential of these epigenome
483 engineering approaches in agricultural settings.

In summary, our work demonstrates that targeted deposition of H3K4me3 is a powerful tool for modulating transcription and meiotic crossover recombination in plants. By deploying both endogenous and orthogonal methyltransferases, we reveal core insights into H3K4me3 function and highlight the potential of this platform for translational application. Future optimisation of guide design, effector choice, and off-target mitigation will be important for enabling both mechanistic discovery and crop engineering through epigenome editing.

491 **METHODS:**

492

493 Plant materials and growth conditions

494 All *Arabidopsis thaliana* lines are in a Col-0 ecotype background. Plants grown on
495 plates were sown on to 1/2x Murashige-Skoog (MS) medium, 1% sucrose and 0.8%
496 agar (pH 5.7), stratified for 2 d at 4 °C in the dark, then transferred to growth chambers
497 (Percival CU-41L4D) at 21 °C under long day light conditions (16 hour light/8 hour
498 dark). Plants grown on soil were grown in F2 soil at 20°C under long day light
499 conditions (16 hour light/8 hour dark). Lines: *rdr6-15* (SAIL_617_H07), and *fwa* lines
500 were previously described [27]. NahG and *edr1* were kindly provided by Prof. Juriaan
501 Ton, previously described in [45]. *bal* lines were previously described in [41]. The CTL 3.9
502 line was previously described in [48,51]. All transgenic plants were generated by
503 *Agrobacterium tumefaciens* strain AGL1 using floral dip [68].

504

505 Plasmid construction

506 To generate the SunTag:SDG2:FWA_g4 construct: the CDS of the catalytic domain of
507 SDG2 (from amino acids 1571-2335) was amplified and coned into into the BsiWI
508 linearised SunTag construct (previously described [28]), using In-Fusion (Takara). To
509 generate dSDG2: the conserved amino acid predicted to abrogate catalytic activity
510 when mutated (Y1903F) was identified using ConSurf [69]. Overlapping PCR was used
511 to generate a version of SDG2 containing the desired mutation (see Supplementary
512 Table 1), and the amplified PCR product was cloned into a BsiWI linearized SunTag-
513 SDG2 construct by In-Fusion (Takara). To generate SunTag:PRDM9, the catalytic
514 domain of mouse PRDM9 (110-417aa) (described in Policarpi et al 2024) was
515 synthesised (TWIST Bioscience) and cloned into the SunTag using the same BsiWI
516 linearization and In-Fusion method described above. Subsequently, overlap PCR was
517 used to generate a version of PRDM9 with the G282A mutation (see Supplementary
518 Table 1). The SNC1 (guides were chosen based on the predicted binding proximity to
519 the TSS), LRCen3, and the no guides controls, were cloned using the protocol
520 described in [70] (see Supplementary Table 1).

521

522 Chromatin Immunoprecipitation

523 The chromatin immunoprecipitation experiments were performed as previously
524 described [71]. 2g of 14-day-old seedlings were collected per biological replicate. For

525 SunTag-SDG2 FWA and SunTag-SDG2 SNC1 input material are pooled T_2 plants. For
526 the SunTag:PRDM9:FWA_g4 in *rdr6*, 2 independent T_3 lines expressing FWA, 2
527 independent T_3 lines NoG were used alongside *rdr6* controls. 7 µl of anti-HA (3F10,
528 Merck) and 5 µl of anti-H3K4me3 (ab8580, abcam) were added to up to 2 ml of
529 sheared chromatin per sample for pulldown. The ChIP purified DNA was directly used
530 for ChIP-qPCR and ChIP-seq library preparation. Primer information is listed in
531 Suppletory Table 1. Values were normalised to Input ($2^{-(\text{ChIP Ct} - \text{Input Ct})}$*100). ChIP-seq
532 libraries were generated using NuGen Ovation Ultra Low System V2 kits according to
533 manufacturer's instructions and were sequenced on an Illumina NovaSeq X
534 instrument with 150bp paired-end reads.
535
536 Crossover measurement
537 For the recombination rate experiment, SunTag plasmids were transformed into F_1
538 plants derived from a cross between the traffic line *CTL3.9* (containing insertions of
539 NAP:eGFP and NAP:dsRED) and Col-0 (Wu et al., 2015). Note that as the red and
540 green T-DNA insertions are separated by nearly 9-Mb, disruption from the T-DNAs
541 insertions (5-Kb and 12-Kb, respectively) are likely to be negligible at this scale [48]. To
542 help reduce the impact of transgene silencing in the absence of the *rdr6* background
543 (due to the impracticality of generating homozygous *rdr6* in the double heterozygous
544 *CTL3.9* F1 background) and to ensure a sufficient number of scorable lines, we aimed
545 to screen 70-100 T_1's per constructs. T_1 transgenic plants (F_2 plants) were recovered
546 on hygromycin selection plates. Seeds harvested from T_1 (F_3) plants were first pre-
547 screened using a Leica DFC310 FX dissecting microscope with ultraviolet filters. Only
548 seeds which contained both red and green markers were cleaned to remove plant
549 debris and included in the analysis pipeline. The seed monolayer containing between
550 1,000 and 2,500 seeds was captured with a Leica DFC310 FX dissecting microscope,
551 first using brightfield followed by UV through a dsRED filter and then UV through a
552 GFP filter. Images were analysed using a modified CellProfiler pipeline (version 4.2.5)
553 described in [48,52,72]. For the F_4 data, seeds derived from the most highly recombining
554 and non-distorted line (P4) were sown (F_3), grown for a generation and seeds from
555 individual plants were collected (F_4) for recombination rate analysis as above, again
556 filtering seed sets from which either of the fluorescent markers had become
557 homozygous (presence / absence) in the previous generation.
558

559 Western blots

560 Western blot were performed as previously described [73] with minor modifications
561 described below. For detection of the large dCAS9-10xGCN4 and SDG2 effector
562 components as shown in Fig S1, single leaf punch (1cm diameter) samples from
563 individual plants were used as input. Tissue was ground in a Tissuelyser II (Retsch)
564 and resuspended in 100 ul of a 60:40 ratio of 2XSDS:8M Urea, mixed, and boiled at
565 95 degrees C for 5 minutes. Samples were centrifuged at >10,000xg to remove debris
566 and loaded into a 3-8% tris acetate gel using MOPS running buffer. After
567 electrophoresis, protein was transferred from the gel to a methanol activated PVDF
568 membrane in Tobin Buffer (25mM Tris, 192mM Glycine, 20% methanol, 0.035% SDS).
569 Membranes were blocked in 5% milk (w/v) in PBST (Phosphate Buffered Saline, 0.1%
570 Tween20) and then incubated with HRP conjugated anti-HA at a 1:3,000 dilution in
571 block. The blot was imaged by ECL detection.

572

573 For the western blots used to detect levels of H3K4me3, 100 mg of 7-day-old seedlings
574 were frozen in liquid nitrogen and ground using a Tissuelyser II (Retsch). Total
575 histones were extracted using the The EpiQuik™ Total Histone Extraction Kit
576 (EpigenTek) according to the manufacturer's instructions. 5 µl of sample for H3 and
577 20 µl of sample for H3K4me3 were loaded onto a NuPage 4-12% BIS-Tris gel
578 (Invitrogen) in NuPage MOPS SDS running buffer (Invitrogen). Transfer from gel to
579 PVDF membrane was performed using an iBlot 3 machine with the dedicated transfer
580 stack (Invitrogen). Following transfer, membrane was blocked in 5% milk (w/v) in TBST
581 (Tris Buffered Saline, 0.1% Tween20) and shaken in room temp for 1 hour. Blocking
582 buffer was discarded and membranes were incubated in primary antibody (anti-H3,
583 ab1791 and anti-H3K4me3, ab8580, Abcam) in blocking buffer (1:1,000) shaking
584 overnight in 4C. Following morning membrane was rinsed in TBST 5 times for 5
585 minutes in room temp. Secondary antibody was added for 1 hour (Goat anti-rabbit
586 HRP, G-21234, Thermo). Membrane was washed again 5 times for 5 minutes.
587 Detection was performed using a SuperSignal West Pico chemiluminescent substrate
588 (#34080, Thermo) using an ImageQuant 800 (Amersham).

589

590 Fluorescent imaging

591 Roots of 7-day-old plants grown in vertical 1/2x MS solid media plates were imaged
592 using a Leica DM6000B epifluorescent microscope.

593

594 Rosette size surface area measurement

595 3-week-old plants grown on soil were imaged using a Google Pixel 7 mounted on a
596 tripod. Images were then analyzed using Fiji.

597

598 *Pseudomonas syringae* colonisation assay

599 Infection assays were performed with *P. syringae* pathovar *tomato* strain DC3000
600 (*Pst*) strain expressing a stable chromosomal insertion of the *lux- CDABE* operon from
601 *Photorhabdus luminescens* (*Pst::LUX*) (Fan et al. 2008), using a slightly modified
602 version of a previously published protocol (Furci et al. 2021). Plants were grown on
603 1/2X MS solid media supplemented with 200 µg/ml Timentin in 96-well plates (Falcon)
604 for 7 days. Prior inoculation, *Pst::LUX* were grown in King's B media containing 50
605 µg/ml Kanamycin and 50 µg/ml Rifampicin overnight at 28 °C. Bacteria were pelleted
606 by centrifugation, washed in 10 mM MgSO4 and finally re-suspended to an OD600 of
607 0.2 in 10 mM MgSO4 containing 0.015% v/v Silwet-L77. 7 days-old seedlings were
608 sprayed with bacteria solution and 96-well plates were sealed with parafilm to maintain
609 100% relative humidity. Seedlings were imaged at 1-4 days post infection (dpi). Prior
610 imaging using (ImageQuant 800, Amersham), plates were left in the dark for 2 mins.
611 Bacterial bioluminescence images were acquired with 4 mins exposure time and bright
612 field images were taken using OD settings of the ImageQuant 800. Image-based
613 quantification of bioluminescence was carried out in Fiji. For each well, the well outline
614 was obtained from bright field images and added to ROI Manager. These ROIs were
615 then transposed onto the bioluminescence images. The bioluminescence intensity
616 from infected seedlings was obtained using the Fiji functions Analyse, Measure and
617 Mean value.

618

619 RT-qPCR

620 RNA was extracted from indicated plant material using TRIzol reagent (Invitrogen) and
621 the Direct-Zol RNA MiniPrep (Zymo) kit, including in-column DNase treatment
622 following the manufacturer's instructions. cDNA was synthesized using SuperScript IV
623 (Invitrogen). qRT-PCRs were performed using a Luna Universal qPCR Master Mix
624 (NEB) and a CFX connect Real-time PCR detection system (Bio-rad). For SunTag-
625 SDG2 targeting FWA and SNC1, RNA was extracted from 14-day-old whole seedlings
626 grown on 1/2x MS plates. SNC1 targeted lines were treated with *Pst::LUX* 4 hours

627 prior to harvesting. For SunTag:PRDM9 qRT-PCR, RNA was extracted from 4 weeks-
628 old leaf tissue of all T_1 lines and 2 independent T_3 lines per construct. 450 ng of total
629 RNA was used for cDNA synthesis. Primers are listed in Supplementary Table 1.
630
631 Quant-Seq Library construction
632 For Suntag-SDG2 QuantSeq, 350 ng of total RNA from ~10 pooled T_2 plants were
633 used as input material. For Suntag:PRDM9 Quant-seq, 350 ng of total RNA from 3 T_1
634 SunTag:PRDM9:FWA_g4 plants expressing FWA, 3 T_1 no guide SunTag:PRDM9
635 lines and *rdr6* and plants was used for library preparation. Libraries were prepared
636 using QuantSeq 3 'mRNA-Seq Library Prep Kit FWD (Lexogen) according to
637 manufacturer's instructions and sequenced on Illumina NovaSeq 6000 PE150
638 instrument.
639
640 Bioinformatic Analysis
641 ChIP-seq analysis
642 The ChIP-seq analysis pipeline was performed as previously described with minor
643 modifications. Bowtie2 (version 2.5.0) was used to map the PE150 bp read data in
644 fastq format to the TAIR10 genome (--no-unal), and were converted to bam format
645 using Samtools (version 1.10). Reads were de-duplicated using the samtools fixmate
646 and markdup commands (see https://github.com/C-Jake-Harris/Binenbaum-SunTag-
647 H3K4me3 for more details). Tracks were generated in DeepTools (version 3.5.1) using
648 bamCoverage (--normalizeUsing RPGC, --effectiveGenomeSize 135000000 --binSize
649 10) with multicopy regions blacklisted (--blackListFileName) using the regions
650 identified in [74]. For analysis of reads mapping to the centromere, a modified version of
651 the previously described pipeline [50] was used. Briefly, PE150 bp read data in fastq
652 format were mapped to the Col-CEN genome [47] using Bowtie2 (version 2.2.5) with (--
653 very-sensitive -k 200 --no-unal --no-discordant) and were filtered for primary
654 alignments using samtools view (-F 256 -q 5) prior to deduplication and track
655 generation, as above. Peaks were called using MACS2 (version 2.2.9.1) with default
656 parameters. multiBigwigSummary (BED-file --outRawCounts) was used to gather
657 normalised read enrichment over called peaks. Correlation plots were generated in
658 DeepTools using MultiBamSummary (--binSize 25) and PlotCorrelation (-c pearson --
659 removeOutliers --plotNumbers -p heatmap).
660

QuantSeq Analysis

In accordance with the manufacturer's (Lexogen) instructions, only read (*1.fq.gz) from PE150 bp data was used for downstream analysis. Briefly, reads were trimmed using cutadapt (version 1.18) and were mapped to the genome using STAR (version 2.7.10b) to the TAIR10 genome (--quantMode GeneCounts --alignIntronMax 10000 --outSAMmultNmax 20). Gene counts were used as input for DESeq2 analysis in R. Differentially expressed genes were defined using an adjusted p-value (Bonferroni method) cutoff of <0.01.

gRNA binding analysis

For the LRCen3 binding and mismatch analysis, the LRCen3 guide RNA sequence (5'-AGGCTTACAAGATTGGGTTG-3'), was mapped to the Col-CEN genome using bowtie2 (version 2.2.5). The following options were used for no mismatches (-f -a --end-to-end --np 0 --score-min L,0,0) and for 1 mismatch (-f -a --end-to-end --score-min L,0,-1). Mapped reads were sorted and converted to bam format using Samtools (version 1.10), and subsequently converted to .bed format using the bamtobed function in bedtools (2.20.1). Bed files were used for downstream analysis in R to generate chromosome-wide density plots over 100kb regions.

Statistics and reproducibility

Statistical significance was determined by using unpaired two-tailed Student's t-test for two-group comparisons and ANOVA with post-hoc Tukey HSD for multiple comparisons. Asterisks indicate significant differences (*$P < 0.05$, **$P < 0.01$, ***$P < 0.001$). Different lowercase letters indicate significant differences ($P < 0.05$). No statistical method was used to predetermine sample size, no data were excluded from the analyses, the experiments were not randomized, and the investigators were not blinded to allocation during experiments and outcome assessment.

DATA AVAILABILITY:

The high-throughput sequencing data generated has been deposited to NCBI (GSE288686 [https://www.ncbi.nlm.nih.gov/geo/query/acc.cgi?acc=GSE288686]. Previously published datasets: CENH3 ChIP-seq and input are on ArrayExpress (E-MTAB-11974, [https://www.ebi.ac.uk/biostudies/arrayexpress/studies/E-MTAB-

11974])[47,50]. Custom scripts used are available on GitHub (https://github.com/C-Jake-Harris/Binenbaum-SunTag-H3K4me3). Source Data are provided with this paper.

698 **REFERENCES:**
699

700 1. Lloyd, J. P. B. & Lister, R. Epigenome plasticity in plants. *Nat. Rev. Genet.* **23**,
701 55–68 (2022).
702 2. Schwaiger, M. *et al.* Evolutionary conservation of the eumetazoan gene
703 regulatory landscape. *Genome Res.* **24**, 639–650 (2014).
704 3. Wang, H. & Helin, K. Roles of H3K4 methylation in biology and disease. *Trends*
705 *Cell Biol.* **xx**, 1–14 (2024).
706 4. Howe, F. S., Fischl, H., Murray, S. C. & Mellor, J. Is H3K4me3 instructive for
707 transcription activation? *BioEssays* **39**, 1–12 (2017).
708 5. Perez, M. F. & Sarkies, P. Histone methyltransferase activity affects metabolism
709 in human cells independently of transcriptional regulation. *PLoS Biol.* **21**, 1–31
710 (2023).
711 6. Vermeulen, M. *et al.* Selective Anchoring of TFIID to Nucleosomes by
712 Trimethylation of Histone H3 Lysine 4. *Cell* **131**, 58–69 (2007).
713 7. Lauberth, S. M. *et al.* H3K4me3 interactions with TAF3 regulate preinitiation
714 complex assembly and selective gene activation. *Cell* **152**, 1021–1036 (2013).
715 8. Wang, H. *et al.* H3K4me3 regulates RNA polymerase II promoter-proximal
716 pause-release. *Nature* **615**, 339–348 (2023).
717 9. Xie, S. S. *et al.* JMJ28 guides sequence-specific targeting of ATX1/2-containing
718 COMPASS-like complex in Arabidopsis. *Cell Rep.* **42**, 112163 (2023).
719 10. Shang, J. Y. *et al.* COMPASS functions as a module of the INO80 chromatin
720 remodeling complex to mediate histone H3K4 methylation in Arabidopsis. *Plant*
721 *Cell* **33**, 3250–3271 (2021).
722 11. Xue, M. *et al.* Single amino acid mutations in histone H3.3 illuminate the
723 functional significance of H3K4 methylation in plants. *Nat. Commun.* **16**, (2025).
724 12. Xiao, J., Lee, U. & Wagner, D. ScienceDirect Tug of war : adding and removing
725 histone lysine methylation in Arabidopsis. *Curr. Opin. Plant Biol.* **34**, 41–53
726 (2016).
727 13. Xu, L. *et al.* H3K4me3 binding ALFIN - LIKE proteins recruit SWR1 for gene -
728 body deposition of H2A . Z. *Genome Biol.* (2025). doi:10.1186/s13059-025-
729 03605-7
730 14. Borde, V. *et al.* Histone H3 lysine 4 trimethylation marks meiotic recombination
731 initiation sites. *EMBO J.* **28**, 99–111 (2009).

732 15. Fayos, I. *et al.* Manipulation of Meiotic Recombination to Hasten Crop
733 Improvement. *Biology (Basel).* **11**, 1–15 (2022).
734 16. Taagen, E., Bogdanove, A. J. & Sorrells, M. E. Counting on Crossovers:
735 Controlled Recombination for Plant Breeding. *Trends Plant Sci.* **25**, 455–465
736 (2020).
737 17. Rowan, B. A. *et al.* An Ultra High-Density Arabidopsis thaliana Crossover.
738 *Genetics* **213**, 771–787 (2019).
739 18. Tock, A. J. *et al.* Crossover-active regions of the wheat genome are
740 distinguished by DMC1, the chromosome axis, H3K27me3, and signatures of
741 adaptation. *Genome Res.* **31**, 1614–1628 (2021).
742 19. Powers, N. R. *et al.* The Meiotic Recombination Activator PRDM9 Trimethylates
743 Both H3K36 and H3K4 at Recombination Hotspots In Vivo. *PLoS Genet.* **12**, 1–
744 24 (2016).
745 20. Choi, K. *et al.* Arabidopsis meiotic crossover hot spots overlap with H2A.Z
746 nucleosomes at gene promoters. *Nat. Genet.* **45**, 1327–1338 (2013).
747 21. Policarpi, C. & Hackett, J. A. Epigenetic editing : Dissecting chromatin function.
748 *BioEssays* 1–16 (2021).
749 22. Villiger, L. *et al.* CRISPR technologies for genome, epigenome and
750 transcriptome editing. *Nat. Rev. Mol. Cell Biol.* (2024). doi:10.1038/s41580-023-
751 00697-6
752 23. Wang, X. & Yamaguchi, N. Cause or effect: Probing the roles of epigenetics in
753 plant development and environmental responses. *Curr. Opin. Plant Biol.* **81**,
754 102569 (2024).
755 24. Dubois, A. & Roudier, F. Deciphering Plant Chromatin Regulation via
756 CRISPR/dCas9-Based Epigenome Engineering. *Epigenomes* **5**, 17 (2021).
757 25. Harris, C. J., Amtmann, A. & Ton, J. Epigenetic processes in plant stress
758 priming : Open questions and new approaches. *Curr. Opin. Plant Biol.* **75**,
759 102432 (2023).
760 26. Tanenbaum, M. E., Gilbert, L. a, Qi, L. S., Weissman, J. S. & Vale, R. D. A
761 versatile protein tagging system for signal amplification in single molecule
762 imaging and gene regulation. *Cell* **159**, 635–646 (2014).
763 27. Wang, M. *et al.* A gene silencing screen uncovers diverse tools for targeted gene
764 repression in Arabidopsis . *Nat. Plants* (2023). doi:10.1038/s41477-023-01362-
765 8

766 28. Papikian, A., Liu, W., Gallego-bartolomé, J. & Jacobsen, S. E. Site-specific
767 manipulation of Arabidopsis loci using CRISPR-Cas9 SunTag systems. *Nat.*
768 *Commun.* **10**, (2019).
769 29. Gallego-Bartolomé, J. *et al.* Targeted DNA demethylation of the *Arabidopsis*
770 genome using the human TET1 catalytic domain. *Proc. Natl. Acad. Sci.* **115**,
771 201716945 (2018).
772 30. Pflueger, C. *et al.* A modular dCas9-SunTag DNMT3A epigenome editing
773 system overcomes pervasive off-target activity of direct fusion dCas9-DNMT3A
774 constructs. *Genome Res.* **28**, 1193–1206 (2018).
775 31. Policarpi, C., Munafò, M., Tsagkris, S., Carlini, V. & Hackett, J. A. Systematic
776 epigenome editing captures the context-dependent instructive function of
777 chromatin modifications. *Nat. Genet.* **56**, 1168–1180 (2024).
778 32. Cheng, Y., Zhou, Y. & Wang, M. Targeted gene regulation through epigenome
779 editing in plants. *Curr. Opin. Plant Biol.* **80**, 102552 (2024).
780 33. Selma, S. & Orzáez, D. Perspectives for epigenetic editing in crops. *Transgenic*
781 *Res.* **30**, 381–400 (2021).
782 34. Guo, L., Yu, Y., Law, J. A. & Zhang, X. Set domain group2 is the major histone
783 H3 lysine 4 trimethyltransferase in Arabidopsis. *Proc. Natl. Acad. Sci. U. S. A.*
784 **107**, 18557–18562 (2010).
785 35. Gardiner, J., Ghoshal, B., Wang, M. & Jacobsen, S. E. CRISPR–Cas-mediated
786 transcriptional control and epi-mutagenesis. *Plant Physiol.* **188**, 1811–1824
787 (2022).
788 36. Du, J. *et al.* Mechanism of DNA methylation-directed histone methylation by
789 KRYPTONITE. *Mol. Cell* **55**, 495–504 (2014).
790 37. Soppe, W. J. *et al.* The late flowering phenotype of fwa mutants is caused by
791 gain-of-function epigenetic alleles of a homeodomain gene. *Mol. Cell* **6**, 791–
792 802 (2000).
793 38. Wang, M. *et al.* Histone H3 lysine 4 methylation recruits DNA demethylases to
794 enforce gene expression in Arabidopsis. *Nat. Plants* **11**, 206–217 (2025).
795 39. Johnson, L. M. *et al.* SRA- and SET-domain-containing proteins link RNA
796 polymerase V occupancy to DNA methylation. *Nature* **507**, 124–128 (2014).
797 40. Wang, M. Y. *et al.* The plant immune receptor SNC1 monitors helper NLRs
798 targeted by a bacterial effector. *Cell Host Microbe* **31**, 1792-1803.e7 (2023).
799 41. Yi, H. & Richards, E. J. Gene duplication and hypermutation of the pathogen

800 Resistance gene SNC1 in the arabidopsis bal variant. *Genetics* **183**, 1227–1234
801 (2009).
802 42. Yi, H. & Richards, E. J. A cluster of disease resistance genes in Arabidopsis is
803 coordinately regulated by transcriptional activation and RNA silencing. *Plant Cell*
804 **19**, 2929–39 (2007).
805 43. Stokes, T. L., Kunkel, B. N. & Richards, E. J. Epigenetic variation in Arabidopsis
806 disease resistance. *Genes Dev.* **16**, 171–182 (2002).
807 44. Yang, L., Wang, Z. & Hua, J. Multiple chromatin-associated modules regulate
808 expression of an intracellular immune receptor gene in Arabidopsis. *New Phytol.*
809 **237**, 2284–2297 (2023).
810 45. Furci, L., Pardo, D. P. & Ton, J. A rapid and non - destructive method for spatial
811 – temporal quantification of colonization by Pseudomonas syringae pv . tomato
812 DC3000 in Arabidopsis and tomato. *Plant Methods* 1–8 (2021).
813 doi:10.1186/s13007-021-00826-2
814 46. Yelina, N. E. *et al.* Epigenetic remodeling of meiotic crossover frequency in
815 Arabidopsis thaliana DNA methyltransferase mutants. *PLoS Genet.* **8**,
816 e1002844 (2012).
817 47. Naish, M. *et al.* The genetic and epigenetic landscape of the Arabidopsis
818 centromeres. *Science (80-.).* **374**, (2021).
819 48. Fernandes, J. B. *et al.* Structural variation and DNA methylation shape the
820 centromere-proximal meiotic crossover landscape in Arabidopsis. *Genome Biol.*
821 **25**, 1–31 (2024).
822 49. Yelina, N. E. *et al.* DNA methylation epigenetically silences crossover hot spots
823 and controls chromosomal domains of meiotic recombination in Arabidopsis.
824 *Genes Dev.* **29**, 2183–2202 (2015).
825 50. Wlodzimierz, P. *et al.* Cycles of satellite and transposon evolution in Arabidopsis
826 centromeres. *Nature* **618**, 557–565 (2023).
827 51. Wu, G., Rossidivito, G., Hu, T., Berlyand, Y. & Poethig, R. S. Traffic lines: New
828 tools for genetic analysis in Arabidopsis thaliana. *Genetics* **200**, 35–45 (2015).
829 52. Kbiri, N., Dluzewska, J., Henderson, I. R. & Ziolkowski, P. A. Quantifying Meiotic
830 Crossover Recombination in Arabidopsis Lines Expressing Fluorescent
831 Reporters in Seeds Using SeedScoring Pipeline for CellProfiler. in *Plant*
832 *Gametogenesis. Methods in Molecular Biology* (ed. Lambing, C.) 121–134
833 (Springer US, 2022). doi:10.1007/978-1-0716-2253-7_10

834 53. Wang, Y. *et al.* The Arabidopsis DREAM complex antagonizes WDR5A to
835 modulate histone H3K4me2/3 deposition for a subset of genome repression.
836 *Proc. Natl. Acad. Sci. U. S. A.* **119**, 1–9 (2022).
837 54. Underwood, C. J. *et al.* Epigenetic activation of meiotic recombination near
838 Arabidopsis thaliana centromeres via loss of H3K9me2 and non-CG DNA
839 methylation. *Genome Res.* **28**, 519–531 (2018).
840 55. Leng, X., Thomas, Q., Rasmussen, S. H. & Marquardt, S. A
841 G(enomic)P(ositioning)S(ystem) for Plant RNAPII Transcription. *Trends Plant*
842 *Sci.* **25**, 744–764 (2020).
843 56. Marquardt, S., Petrillo, E. & Manavella, P. A. Cotranscriptional RNA processing
844 and modification in plants. *Plant Cell* **35**, 1654–1670 (2023).
845 57. Rickels, R. *et al.* Histone H3K4 monomethylation catalyzed by Trr and
846 mammalian COMPASS-like proteins at enhancers is dispensable for
847 development and viability. *Nat. Genet.* **49**, 1647–1653 (2017).
848 58. Fal, K., El Khoury, S., Le Masson, M., Berr, A. & Carles, C. C. CRISPR/dCas9-
849 targeted H3K27me3 demethylation at the CUC3 boundary gene triggers ectopic
850 transcription and impacts plant development. *iScience* **28**, 112475 (2025).
851 59. Cuimei Zhang, Yajun Tang, Shanjie Tang, Lei Chen, Haidi Yuan, Yujun Xu,
852 Yangyan Zhou, Shuaibin Zhang, Jianli Wang, Hongyu Wen, Wenbo Jiang,
853 Yongzhen Pang, Xian Deng, Xiaofeng Cao, Junhui Zhou, Xianwei Song, Q. L.
854 P. An Inducible CRISPR-activation tool for accelerated plant regeneration
855 Cuimei. *Plant Commun.* (2024).
856 60. Song, X. *et al.* Inheritance of acquired adaptive cold tolerance in rice through
857 DNA methylation. *Cell* 1–12 (2025). doi:10.1016/j.cell.2025.04.036
858 61. Oberkofler, V. & Bäurle, I. Inducible epigenome editing probes for the role of
859 histone H3K4 methylation in Arabidopsis heat stress memory. *Plant Physiol.*
860 703–714 (2022). doi:10.1093/plphys/kiac113
861 62. Casas-Mollano, J. A., Zinselmeier, M. H., Sychla, A. & Smanski, M. J. Efficient
862 gene activation in plants by the MoonTag programmable transcriptional
863 activator. *Nucleic Acids Res.* **51**, 7083–7093 (2023).
864 63. Pan, C. *et al.* CRISPR–Act3.0 for highly efficient multiplexed gene activation in
865 plants. *Nat. Plants* **7**, 942–953 (2021).
866 64. de Melo, B. P. *et al.* Transcriptional modulation of AREB-1 by CRISPRa
867 improves plant physiological performance under severe water deficit. *Sci. Rep.*

868 **10**, 1–10 (2020).
869 65. Boone, B. A. *et al.* ACD15, ACD21, and SLN regulate the accumulation and
870 mobility of MBD6 to silence genes and transposable elements. *Sci. Adv.* **9**, 1–
871 14 (2023).
872 66. Baldini, A., Battaglia, F. & Perrella, G. The generation of novel epialleles in
873 plants: the prospective behind re-shaping the epigenome. *Front. Plant Sci.* **16**,
874 (2025).
875 67. Lu, Z. *et al.* The prevalence, evolution and chromatin signatures of plant
876 regulatory elements. *Nat. Plants* **5**, 1250–1259 (2019).
877 68. Clough, S. J. & Bent, A. F. Floral dip: A simplified method for Agrobacterium-
878 mediated transformation of Arabidopsis thaliana. *Plant J.* **16**, 735–743 (1998).
879 69. Ashkenazy, H. *et al.* ConSurf 2016: an improved methodology to estimate and
880 visualize evolutionary conservation in macromolecules. *Nucleic Acids Res.* **44**,
881 W344–W350 (2016).
882 70. Ghoshal, B. & Gardiner, J. CRISPR-dCas9-Based Targeted Manipulation of
883 DNA Methylation in Plants. *Springer Protoc. Handbooks* **2**, 57–71 (2021).
884 71. Harris, C. J., Zhong, Z., Ichino, L., Feng, S. & Jacobsen, S. E. H1 restricts
885 euchromatin-associated methylation pathways from heterochromatic
886 encroachment. *Elife* 1–17 (2024).
887 72. Gorringe, N., Topp, S., Burns, R., Yamaguchi, S. & Fernando, A. Natural
888 variation modifies centromere-proximal meiotic crossover frequency and
889 segregation distortion in Arabidopsis thaliana. *bioRxiv* 1–69 (2025).
890 73. Ichino, L. *et al.* MBD5 and MBD6 couple DNA methylation to gene silencing
891 through the J-domain protein SILENZIO. *Science (80-.).* **1439**, 1434–1439
892 (2021).
893 74. Klasfeld, S., Roulé, T. & Wagner, D. Greenscreen: A simple method to remove
894 artifactual signals and enrich for true peaks in genomic datasets including ChIP-
895 seq data. *Plant Cell* **34**, 4795–4815 (2022).
896 75. Abramson, J. *et al.* Accurate structure prediction of biomolecular interactions
897 with AlphaFold 3. *Nature* **630**, 493–500 (2024).
898

ACKNOWLEDGEMENTS

We would like to thank Jurriaan Ton's group at the University of Sheffield for their generous gift of the *Pst::LUX* strain, and for their support in helping to establish the infection and quantification protocol in the Harris group. **Funding:** C.J.H. is supported by a Royal Society University Research Fellowship (URF\R1\201016) and an ERC Starting Grant (TransPlantMemory), funded by UKRI EPSRC (EP/X025306/1). J.B. is supported by a Marie Curie postdoctoral fellowship, funded by UKRI (EP/Z001749/1). V.A. is supported by a 4-year BBSRC-funded doctoral studentship. I.R.H is supported by UKRI/BBSRC grants BB/Y009487/1 and BB/V003984/1, and an ERC Advanced Grant (EvoPanCen). N.G. is supported by a BBSRC-UKRI doctoral studentship. S.E.J. is an investigator of the Howard Hughes Medical Institute.

AUTHOR CONTRIBUTIONS

C.J.H., I.R.H. and S.E.J. conceived, designed and supervised the research. C.J.H. performed experiments, NGS bioinformatic analysis, and assembled the manuscript. J.B. performed the majority of the experiments relating to SunTag:SDG2. V.A. performed the experiments relating to SunTag:PRDM9. H.F. performed the majority of experiments and analysis relating to meiotic recombination. L.X. performed the SunTag:SDG2 centromere-targeting ChIP-seq. N.G. provided the Col-0 x *CTL3.9* F_1 seeds and guidance on the analysis of recombination frequency. P.W. and R.B. contributed to the design of the centromere targeting guide RNA. A.P. cloned SDG2 into SunTag.

COMPETING INTERESTS

The authors declare no competing interests.